BER Analysis of Coherent Free Space Optical Communication Systems with Holographic Modal Wavefront Sensor

Wei Liu[1], Kainan Yao[2], Danian Huang[1]*, Jingtai Cao[2,3], Liang Wang[2], and Haijun Gu[3]

[1]College of Geoexploration Science and Technology, Jilin University, 938, West Democracy Street, Changchun, Jilin 130026, China
[2]Changchun Institute of Optics, Fine Mechanics and Physics, Chinese Academy of Sciences,3888 Nanhu Road, Changchun 130033, China
[3]College of communication Engineering, Jilin University, 5372 Nanhu Road, Changchun 130012, China

Degradation of bit-error-rate (BER), caused by atmospheric turbulence, seriously hinders the performance of coherent Free Space Optical (FSO) communication systems. An adaptive optics system proves to be effective in suppressing the atmospheric turbulence. The holographic modal wavefront sensor (HMWFS) proposed in our previous work, noted for its fast detecting rates and insensitivity to beam scintillation, is applied to the coherent FSO communication systems. In this paper, based on our previous work, we first introduce the principle of the HMWFS in brief and give the BER of the coherent FSO with homodyne detection in theory, and then analyze the improvement of BER for a coherent FSO system based on our previous simulation works. The results show that the wavefront sensor we propose is better for weak atmospheric turbulence. The most obvious advantages of HMWFS are fast detecting rates and insensitivity to beam scintillation.

Keywords : BER, Coherent FSO communication, Holographic modal wavefront sensor, Aberrations correction
OCIS codes : (010.1080) Active or adaptive optics; (060.0060) Fiber optics and optical communications; (060.4510) Optical communication

I. INTRODUCTION

For the free space optical communication (FSO) system, the performance of the coherent detection scheme is better than that of the intensity modulation direct detection, with higher spectral efficiencies and data rates, a greater ability to decrease both background and thermal noise, and more sensitive receivers [1-4]. However, the atmospheric turbulence greatly degrades the performance of the coherent FSO systems [5]. The wavefront distortion, scintillation, beam wandering and spreading caused by a turbulent atmosphere will not only degrade the entrance efficiency of the receiving antenna but also cause mismatch of the field of the signal beam and the local oscillator (LO) [6].

An adaptive optics (AO) system is identified as an effective way to compensate atmospheric turbulence in a coherent FSO system [7, 8]. And as the main component of an AO system, the wavefront sensor is attracting extensive attention [9]. The Shack-Hartmann wavefront sensor (SHWFS) is widely used for turbulence compensation for a coherent FSO system [10]. Belmonte put emphasis on elucidating how the addition of AO to the transmitter or receiver can reduce the effects of atmospheric propagation and on quantifying the improvement on the performance of FSO systems regarding coherent detection [11, 12]. Zuo investigated the bit-error-rate (BER) performance of the FSO links in weak non-Kolmogorov turbulence and showed that BER decreased sharply with AO corrections. Considering the influence of both the amplitude fluctuation and spatial phase aberrations, when the ratio of receiving aperture diameter D to the coherent length r_0 (D/r_0) was large enough, the Zernike mode was accurate [13, 14]. Li evaluated the performance of the coherent FSO system employing quad-

rature array phase-shift keying modulation over the maritime atmosphere with AO system based on SHWFS for atmospheric turbulence compensation [15]. C. Liu and J. Huang analyzed the improvement of BER for the coherent FSO system with AO system based on SHWFS through numerical simulation and experimental data of the 1.8 m telescope with a 127-subaperture SHWFS, under different D/r_0 [16-19]. However, the SHWFS was so sensitive to laser scintillation that the performance was limited seriously for a coherent FSO system. The focal plane wavefront sensor solved this problem. It had higher power usage ratio, but it was much more costly in time [20]. In 2000, Ghebremichael et al. applied computer-generated holographic elements to wavefront sensing and corrected the response curve [21-25]. Changhai et al. used the plane wave in combination with the Fourier lens for the replacement of spherical waves to improve the efficiency of energy utilization [26-28].

In this paper, based-on our previous work, HMWFS is applied to the coherent FSO systems to evaluate the BER performance improvement. First, the principle of HMWFS and the BER of the coherent FSO communication are given in brief in Section 2. Then, the numerical simulation is used to verify the feasibility of the HMWFS for the coherent FSO system, and the BER improvement for the coherent FSO system with HMWFS based on our previous works are presented in Section 3. Finally, we summarize and present our conclusions in Section 4.

II. THEORETICAL ANALYSIS

2.1 The holographic modal wavefront sensing

The theoretical layout of HMWFS is shown in Fig. 1 [29].

An object beam with the minimum expected amplitude of the aberration $A_{\min}Z_i$ and a reference beam focused at point A on a distant detector record one hologram, as shown in Fig. 1(a). Another hologram is recorded by an object beam with the maximum amplitude of the aberration $A_{\max}Z_i$ and a reference beam focused at a different point B, as shown in Fig. 1(b). Then a multiplexed hologram is generated with the pair of holograms [29].

The hologram will be reconstructed with an input beam with some amplitude, A_i, which is between the maximum and minimum values, The beams will be focused at point A and point B, as shown in Fig. 1(c). The relative intensity of at these points is related to the coefficient of Zernike item. Thus, after a calibration, the amplitude can be obtained simply by sensing the spot intensities.

In addition, the multiplexed hologram with more pairs of holograms is needed to increase the number of aberration modes detected. Considering the pairs of spots are spatially separate, the amplitudes of these spots can be read out in parallel by a sensor array. Thus, the Zernike modal amplitude can be obtained through comparing the relative intensities of pairs of spots [29].

According to Fourier optics, suppose the amplitude of the signal beam is $U_{S,0}$, the phase function is $\phi(r_s)$, then the complex amplitude of the signal beam can be expressed as:

$$U_S(r) = U_{S,0} \exp[i\phi(r_s)] \tag{1}$$

And the complex amplitude of the reference beam can be expressed as:

$$U_R(r) = U_{R,0} \exp[i\phi(r_R)] \tag{2}$$

Where, $U_{R,0}$ is the amplitude of the reference beam, and $\phi(r_R)$ is the phase function of the reference beam.

The two waves interfere on the recording medium, and generate a holographic pattern. When a replay beam with random aberrations illuminates the holographic pattern, the wavefront of the signal beam can be reconstructed on the focal plane. The diffraction field distribution on the focal plane shall be expressed as [29]:

$$U_d(r_d) = \int (U_S^* U_R + c.c) U_P(r_P, r) G(r_d, r) dr \tag{3}$$

Where $c.c$ is a constant, U_S^* is the conjugate of $U_S(r)$, $U_P(r_P, r)$ is the replay beam, and the $G(r_d, r)$ is the Green's
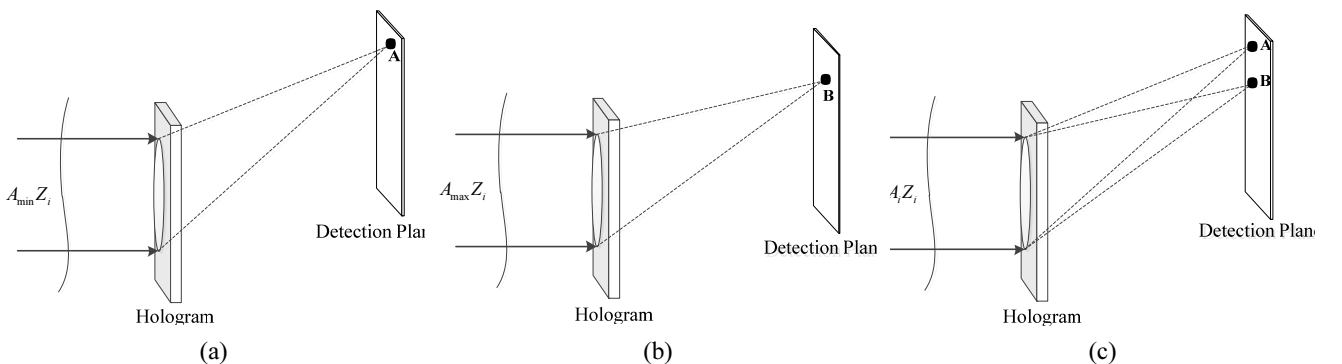

FIG. 1. The theory of HMWFS.

Function. In free space, $G(r_d, r)$ can be approximately expressed as:

$$G(r_d, r) = \frac{\exp\{ik_d[(x_d - x)^2 + (y_d - y)^2 + (z_d - z)^2]^{1/2}\}}{z_d}$$

(4)

Where, k_d is the wave vector of laser beam $U_d(r_d)$ and (x_d, y_d, z_d), (x, y, z) are space coordinates.

Assume the Fresnel approximation conditions are satisfied, the thickness of the hologram is ignored, and $\lambda = \lambda_S = \lambda_P = \lambda_d$, $U_d(r_d)$ can be expressed as [29]:

$$
\begin{aligned}
U_d(r_d) &\approx \exp(i\pi \frac{x_d^2 + y_d^2}{\lambda z}) \iint \exp\left[-i\pi \frac{(x_R - x)^2 + (y_R - y)^2}{\lambda z}\right] \\
&\quad \exp(i\pi \frac{x^2 + y^2}{\lambda z}) \times \exp[-iW(x, y)] \prod(x - a, y - b) U_P(x_P, y_P) \\
&\quad \times \exp(-i2\pi \frac{xx_d + yy_d}{\lambda z}) dxdy \\
&\approx \exp(i\pi \frac{x_d^2 + y_d^2}{\lambda z}) \times F\left\{ \exp\left[-i\pi \frac{(x_R - x)^2 + (y_R - y)^2}{\lambda z}\right] \right. \\
&\quad \exp[-iW(x, y)] \times \prod(x - a, y - b) U_P(x_P, y_P) \\
&\quad \left. \exp(i\pi \frac{x^2 + y^2}{\lambda z}) \right\}_{f_x = \frac{x_d}{\lambda z}, f_y = \frac{y_d}{\lambda z}}
\end{aligned}
$$

(5)

Where, $\prod$ is the pupil function, and the range of integration is limited within the pupil. a and b are respectively the length and width of the hologram. $F\{.\}$ is the Fourier transform. Thus, the Fresnel integral is simplified into a Fourier transform with thin hologram conditions. Thus, the distribution of complex amplitude on the holographic plane can be solved by a numerical method.

2.2 The BER of the coherent FSO system

As mentioned in our previous work, for a coherent FSO system, the received beam is mixed with an LO signal. The received beam and the LO signal are given by [16]:

$$E_S = U_S(r, \varphi) \cos[\omega_S t + \psi_S + \psi_S(r, \varphi)]$$ (6)

$$E_{LO} = U_{LO}(r, \varphi) \cos[\omega_{LO} t + \psi_{LO} + \psi_{LO}(r, \varphi)]$$ (7)

where, $U_S(r, \varphi)$ and $U_{LO}(r, \varphi)$ are the amplitudes of received beam and LO signal. $\psi_S(r, \varphi)$ and $\psi_{LO}(r, \varphi)$ are the variable phases related to spatial position of the laser carrier and LO signal, respectively. ω_S and ω_{LO} are their angular frequencies, respectively. The current after frequency mixing is given by:

$$i = c\int_\sigma \eta \left(E_T \times H_T\right) ds$$ (8)

where H_T is the magnetic field distribution after frequency mixing, $E_T \times H_T$ is the Poynting vector, η is the quantum efficiency of the detector, c is constant, and σ is the area of the detector.

Since the intensity of the LO signal is much larger than the intensity of the received beam, the detector noise is mainly shot noise. Thus, the mean square value of the noise current is given by [16]:

$$\left\langle i_N^2 \right\rangle = 2eI_{LO}B = \left(\frac{c\varepsilon_0 e^2 \eta}{h\nu}\right) B \int_0^{2\pi} \int_0^{r_0} \left[U_{LO}(r, \varphi)\right]^2 rdrd\varphi$$

(9)

where B is the noise bandwidth of the detector, and I_{LO} is the direct current coursed by the LO signal. The signal to noise ratio (SNR) is defined by the ratio of the mean square value of the intermediate frequency signal current and the mean square value of the noise current [16]:

$$SNR = \frac{\left\langle i_h^2 \right\rangle}{\left\langle i_N^2 \right\rangle} = \left(\frac{\eta P_S}{h\nu B}\right) \frac{\left|\int_0^{2\pi} \int_0^{r_0} U_S(r, \varphi) U_{LO}(r, \varphi) \exp[i\Delta\psi(r, \varphi)] rdrd\varphi\right|^2}{\int_0^{2\pi} \int_0^{r_0} \left[U_{LO}(r, \varphi)\right]^2 rdrd\varphi \int_0^{2\pi} \int_0^{r_0} \left[U_S(r, \varphi)\right]^2 rdrd\varphi}$$

(10)

where P_S is the laser signal power. Specially, when $\omega_{IF} = 0$, which is considered as homodyne detection, we can obtain mixing efficiency as [16]:

$$\gamma_{zh} = \frac{\left|\int_0^{2\pi} \int_0^{r_0} U_S(r, \varphi) U_{LO}(r, \varphi) \cos[\Delta\psi(r, \varphi)] rdrd\varphi\right|^2}{\int_0^{2\pi} \int_0^{r_0} \left[U_{LO}(r, \varphi)\right]^2 rdrd\varphi \int_0^{2\pi} \int_0^{r_0} \left[U_S(r, \varphi)\right]^2 rdrd\varphi}$$

(11)

According to the Eq. (12), the mixing efficiency is related to both the amplitude of received beam and LO signal, and spatial phase distribution difference. Assuming the received beam and the LO signal are plane waves with uniform intensity, the mixing efficiency is influenced directly by the spatial phase distribution difference. The AO technology is generally regarded as an effective way to decrease the spatial phase distribution difference between the carrier signal and the LO signal.

In the coherent detection system, the BER can be given by [16]:

$$BER = \frac{1}{2} erfc(\frac{Q}{\sqrt{2}})$$ (12)

where $erfc$ is the complementary error function, $Q = \sqrt{SNR}$. For synchronous binary phase shift keying (BPSK) modulation, the optical power of the received beam is expressed as:

$$P_S = N_P h\nu B \qquad (13)$$

where N_p is the number of photons received within a single bit. For the BPSK modulation, the BER of the homodyne detection can be given as [16]:

$$BER_{zh} = \frac{1}{2} erfc\left(\sqrt{2\eta N_P \gamma_{zh}}\right) \qquad (14)$$

III. NUMERICAL SIMULATION

Based on our previous work, in terms of the computer-generated holograph, the center wavelength of the laser is $\lambda = 632.8$ nm, the number of sampling points of the holographic grating is 600×600 pixels, the aperture of holographs is 60 mm, the distance between image plane and holographic plane is 1500 mm, the off-axis distance of the spot on focal plane is larger than 1 cm. The low eight order Zernike aberrations (Z3, Z4, …, Z10) are coded in this simulation. Where the peak-to-valley (PV) value of Z3, Z4, Z5 is $\lambda / 2$, and the PV value of Z6, Z7, Z8, Z9, Z10 is $\lambda / 4$. The holograph we eventually obtained is shown in Fig. 2 [29].

According to the theory of the HMWFS, the relative intensity distribution on the holographic image plane is shown in Fig. 3 [29]. By comparing the relative intensity on the holographic image plane, the Zernike aberrations are obtained quantitatively.
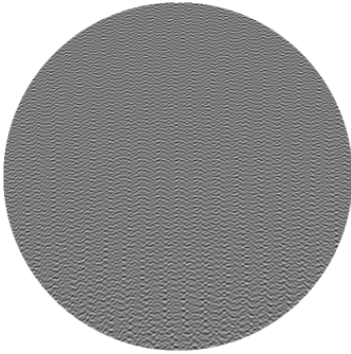

FIG. 2. Computer-generated holograph.

FIG. 3. The spots on holographic image plane.

The mixing efficiency is approximate to the Strehl ratio of the far field of the received beam for homodyne detection, and it is defined by the ratio of the far field encircled energy and the diffraction limited encircled energy [18]. The intensity distribution on the focal plane before correction (detail view) is shown in Fig. 4.

Thus, it can be seen that the holographic modal wavefront sensor has smaller residual in low eight orders Zernike aberrations detection. The intensity distribution on focal plane after aberrations correction is shown in Fig. 5.

Then, we analyze the BER before and after aberrations correction based on Eq. (14) when $N_p = 10$ and $\eta = 1$. The results are shown in Table 1.

We make another five groups numerical simulation by changing the introduced aberrations. In our simulation, we introduce the Zernike mode aberrations into the laser beam before correction. The root-mean-square (RMS) values of the aberrations before correction are between 0.15λ and 0.25λ. And RMS values of the residual aberrations after correction are nearly below 0.1λ [29]. Thus, we get the five images before and after correction as shown in Fig. 6.

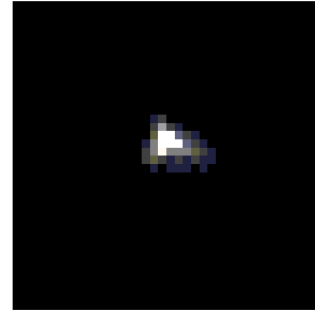Where, the Fig. 6(a) shows the images before correction,

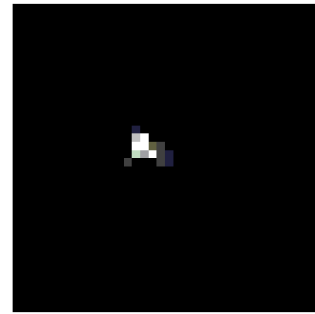FIG. 4. The intensity distribution on focal plane before correction.

FIG. 5. The intensity distribution on focal plane before correction.

TABLE 1. The BER before and after aberrations correction

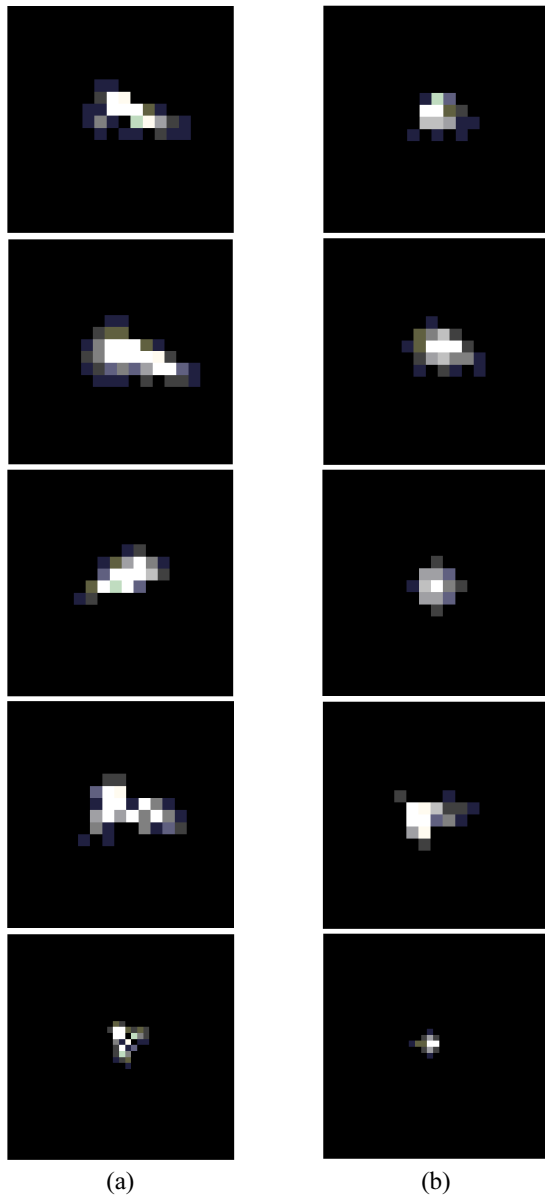| BER before correction with homodyne detection	BER after correction with homodyne detection
2.44×10^{-2}	9.41×10^{-7}

(a)   (b)

FIG. 6. The results of the six groups simulation.

Table 2. The BER of the six groups simulation results

No.	BER Before Correction	BER Before Correction
1	2.44×10^{-2}	9.41×10^{-6}
2	3.52×10^{-2}	1.30×10^{-5}
3	2.82×10^{-4}	1.95×10^{-8}
4	1.50×10^{-3}	4.89×10^{-7}
5	3.26×10^{-4}	2.71×10^{-8}
6	3.78×10^{-4}	1.02×10^{-7}

According to Table 2, we can also verify that the wavefront sensing we proposed is better for weak atmospheric turbulence with fast detecting rates and insensitivity to beam scintillation.

IV. CONCLUSION

In this paper, we analyzed the principle of HMWFS in theory and gave the BER expression of the coherent FSO system, and then first applied HMWFS to a coherent FSO system, and then we analyze the BER performance improvement through numerical simulation based on HMWFS. Finally, we discussed the impact of HMWFS on BER of the coherent FSO system before and after the aberrations correction based on HMWFS. According to the results of numerical simulation, the wavefront sensor we proposed is better for weak atmospheric turbulence. The most obvious advantage of HMWFS is fast detecting rates and insensitivity to beam scintillation.

The disturbance strength is only described by the value of the introduced aberrations in our work. The relationship between the introduced aberrations and the structure constant of refractive index C_n^2 will be carried out in the near future.

and the Fig. 6(b) shows the images after correction. The BER before and after correction are shown in Table 2.

As shown in Table 2, according to homodyne detection coherent FSO system, we can see that before correction, the BER is above 10^{-4}, and after correction, the BER is below 10^{-5}. According to the BER before correction, we can estimate the atmospheric turbulence intensity. Under some weak atmospheric turbulence conditions, the BER is about 10^{-4} before correction. And after AO correction based on HMWFS, the BER can reach below 10^{-7}. In the meanwhile, under some strong atmospheric turbulence conditions, the BER is about 10^{-2} before correction. And after correction, the BER can achieve below 10^{-5}. Above all, the AO system based on HMWFS is an effective way to improve the BER performance of a coherent FSO system with homodyne detection conditions.

REFERENCES

1. L. Wei, Y. Kainan, H. Danian, L. Xudong, W. Liang, and L. Yaowen, "Performance evaluation of coherent free space optical communications with a double-stage fast-steering-mirror adaptive optics system depending on the Greenwood frequency," Opt. Express **24**, 13288-13302 (2016).
2. J. Ma, K. Li, L. Tan, S. Yu, and Y. Cao, "Performance analysis of satellite-to-ground downlink coherent optical communications with spatial diversity over Gamma-Gamma atmospheric turbulence," Appl. Opt. **54**, 7575-7585 (2015).

3. D. Geng, P. Du, W. Wang, G. Gao, T. Wang, and M. Gong, "Single laser free-space duplex communication system with adaptive threshold technique and BER analysis in weak turbulent atmosphere," Opt. Letters **39**, 3950-3953 (2014).

4. R. M. Rennie, D. Goorskey, M. R. Whiteley, and E. J. Jumper, "Wavefront measurements of a laser-induced break-down spark in still air," Appl. Opt. **51**, 2306-2314 (2012).

5. W. Liu, W. Shi, J. Cao, Y. Lv, K. Yao, S. Wang, J. Wang, and X. Chi, "Bit error rate analysis with real-time pointing errors correction in free space optical communication system," Optik **12**, 324-328 (2014).

6. S. Dongyiel, H. Y. Such, and C. J. Woo, "4×10 Gb/s terrestrial optical free space transmission over 1.2 km using an EDFA preamplifier with 100 GHz channel spacing," Opt Express, **7**, 280-284 (2000).

7. Q. Yang, J. Zhao, M. Wang, and J. Jia, "Wavefront sensor-less adaptive opitcs based on the trust region method," Opt. Letters **40**, 1235-1237 (2015).

8. J. Cao, X. Zhao, Z. Li, W. Liu, and Y. Song, "Stochastic parallel gradient descent laser beam control algorithm for atmospheric compensation in free space optical communi-cation," Optik **125**, 6142-6147 (2014).

9. H. Linhai and C. Rao, "Wavefront sensor-less adaptive optics: a general model-based approach," Opt. Express **19**, 371-379 (2011).

10. J. Ma, F. Zhao, L. Tan, S. Yu, and Y. Yang, "Degradation of single-mode fiber coupling efficiency due to localized wavefront abrerrations in free-space laser communications," Opt. Eng. **49**, 1-6 (2010).

11. A. Belmonte, A. Rodríguez, F. Dios, and A. Comeón, "Phase compensation considerations on coherent, free-space laser communications system," Proc. SPIE, **6736**, A-11 (2007).

12. A. Belmonte, "Influence of atmospheric phase compensation on optical heterodyne power measurements," Opt. Express **16**, 6756-6767 (2008).

13. L. Zuo, Y. Ren, A. Dang, and G. Hong, "Performance of coherent BPSK systems using phase compensation and diversity techniques," in Proceedings of IEEE Conference on Global Telecommunications, 1-5 (2010).

14. L. Zuo, A. Dang, Y. Ren, and H. Guo, "Performance of phase compensated coherent free space optical communi-cations through non-Kolmogorov turbulence," Opt. Commun. **28**, 1491-1495 (2011).

15. M. Li and M. Cvijetic, "Coherent free space optics communi-cations over the maritime atmosphere with use of adaptive optics for beam wavefront correction," Appl. Opt. **54**, 1453-1462 (2015).

16. C. Liu, S. Chen, X. Li, and H. Xian, "Performance evaluation of adaptive optics for atmospheric coherent laser communi-cations," Opt. Express, **22**, 15554-15563 (2014).

17. C. Liu, M. Chen, S. Chen, and H. Xian, "Adaptive optics for the free-space coherent optical communications," Opt. Commun. **361**, 21-24 (2016).

18. H. Jian, D. Ke, L. Chao, Z. Peng, J. Dagang, and Y. Zhoushi, "Effectiveness of adaptive optics system in satellite-to-ground coherent optical communication," Opt. Express, **22**, 16000-16007 (2014).

19. J. Huang, H. Mei, K. Deng, L. Kang, W. Zhu, and Z. Yao, "Signal to noise ratio of free space homodyne coherent optical communication after adaptive optics compensation," Opt. Commun. **356**, 574-577 (2015).

20. W. Liu, W. Shi, B. Wang, K. Yao, Y. Lv, and J. Wang, "Free space optical communication performance analysis with focal plane based wavefront measurement," Opt. Commun. **309**, 212-220 (2013).

21. F. Ghebremichael, G. P. Andersen, and Kenneth S. Gurley, "Holography-based wave-front sensing," Appl. Opt. **47**, A62-A69 (2008).

22. G. P. Andersen, L. Dussan, F. Ghebremichael, and K. Chen, "Holographic wave-front sensor," Opt. Eng. **48**, 085801 (2009).

23. G. P. Andersen, F. Ghebremichael, and K. S. Gurley, "Fast Computing-Free Wave-front Sensing," Adaptive Optics: Methods, Analysis and Applications **18**, AWC4 (2007).

24. S. K. Mishra, R. Bhatt, D. Mohan, A. K. Gupta, and A. Sharma, "Differential modal Zernike wavefront sensor emplo-ying a computer-generated hologram: a proposal," Appl. Opt. **48**, 6458-6465 (2009).

25. R. Bhatt, S. K. Mishra, D. Mohan, and A. K. Gupta, "Direct amplitude detection of Zernike modes by computer-generated holographic wavefront sensor: Modeling and simulation" Optics and Lasers in Engineering, **46**, 428-439 (2008).

26. L. Changhai and J. Zongfu, "Holographic Modal Wave-front Sensor: Theoretical Analysis and Simulation," Chinese Journal of Lasers **36**, 147-152 (2009).

27. L. Changhai, X. Fengjie, M. Haotong, H. Shengyang, and J. Zongfu, "Modal wave-front sensor based on binary phase-only multiplexed computer-generated hologram," Appl. Opt. **49**, 5117-5124 (2010) .

28. L. Changhai, X. Fengjie, H. Shengyang, and J. Zongfu, "Performance analysis of multiplexed phase computer-generated hologram for modal wave-front sensing," Appl. Opt. **50**, 1631-1639 (2011).

29. W. Liu, W. Shi, K. Yao, J. Cao, P. Wu, and X. Chi, "Fiber Coupling efficiency analysis of free space optical communi-cation systems with holographic modal wavefront sensor," Opt. Laser Technol. **60**, 116-123 (2014).